Proceedings of the 15th International Middle East Power Systems Conference (MEPCON'12), Alexandria University, Egypt, December 23-25, 2012, Paper ID 212.

Low-Cost Stand-Alone Wind System with Battery Storage Using Doubly-Fed Induction Generator

O. E. M. Youssef
Faculty of Engineering at Shoubra, Benha University, Cairo, Egypt
omsamoh@yahoo.com

A. Shaltout
Faculty of Engineering, Cairo University, Giza, Egypt
aashaltout@yahoo.com

***Abstract* - It is proposed to employ doubly-fed induction generator (DFIG) in stand-alone wind system with battery storage. The proposed system is of low cost compared with the traditional system. Pulse-width modulation (PWM) converter is controlled to ensure maximum power extraction through the DFIG operation, provided that the battery bank is not overcharged, and to provide the reactive power required by the DFIG from the battery bank. Simulation results are provided in the paper for various operating conditions to demonstrate the capability of the system.**

Index Terms* - *Stand-alone wind system, doubly-fed induction generator, battery bank, pulse-width modulation converter.

I. INTRODUCTION

Renewable energy sources, such as wind energy and photovoltaic energy, are used in stand-alone systems supplying remote houses. These sources are of intermittent nature and, therefore, the stand-alone systems include storage battery banks. The storage battery banks improve the reliability of these systems because the excess energy is stored in the battery bank, and this energy is delivered to the load when the available energy is not sufficient.

The traditional configuration of stand-alone wind system with battery storage (residential wind system) has a permanent-magnet synchronous generator (PMSG) [1]–[4]. There is a maximum voltage limit of the battery bank to protect the battery bank against overcharging [4]–[7]. Therefore, it is required to capture the maximum power from the wind turbine provided that the maximum voltage limit is not exceeded [4]. Terminals of PMSG are usually connected to diode bridge rectifier and DC/DC converter [2], [3]. The required operation can be obtained by controlling the duty ratio of the DC/DC converter [3]. An alternative system has a controlled rectifier and a wind turbine with flexible blades. Optimal performance is obtained by twisting of the turbine blades, and the firing angle of the rectifier is kept at zero value while the battery voltage is less than the maximum voltage limit [4].

PMSG can be used in the system with gearless drive. However, PMSG is expensive and heat sensitive. In many cases, induction generators with single-stage gearbox may be less expensive [8]. In [9], the authors have replaced the PMSG with squirrel-cage induction generator in the stand-alone system. In this system, the cost of the converter has been increased since it carries both the full active and reactive powers. This increase may overcome the cost saving of using the squirrel-cage induction generator.

In this paper, it is recommended to use doubly-fed induction generator (DFIG) which provides saving in the converter size and results in a reduction in the overall cost. The proposed system is shown in Fig. 1. The PWM converter is controlled to provide the reactive power required by DFIG. Also, the PWM converter is controlled to capture the maximum power from the wind turbine, where this power must not exceed the rated power of the wind turbine, provided that the maximum voltage limit (U_{max}) of the battery bank is not exceeded. Different results are obtained to examine the performance of the system.

II. CHARACTERISTICS OF WIND TURBINE

The developed mechanical power of a turbine rotor is given by [10]–[12]:

$$P_m = \frac{1}{2} C_p \, \rho A V_w^{\,3} \tag{1}$$

where C_p is the power coefficient, ρ is the air density, V_w is the wind speed and A is the area swept by the wind turbine. The swept area is give by

$$A = \pi R^2 \tag{2}$$

where R is the radius of the turbine rotor.
The power coefficient is given as a function of tip-speed ratio (α). The relationship between α and C_P of a wind turbine is given in Fig. 2, where α is given by

$$\alpha = \frac{\text{tip speed of rotor blades}}{\text{wind speed}} = \frac{\omega R}{V_w} \tag{3}$$

where ω is the angular velocity of the turbine shaft.
The mechanical power (P_m) against the turbine speed is shown in Fig. 3. This figure shows that to maximize the extracted

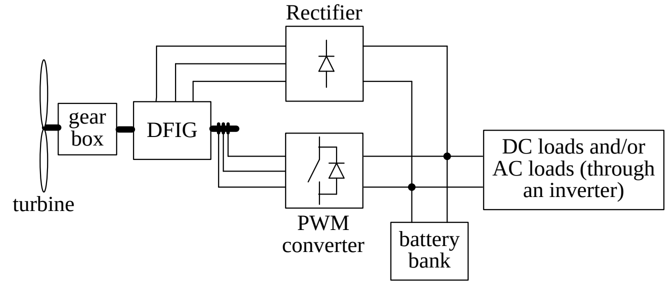

Fig. 1 Proposed configuration of stand-alone residential wind system.

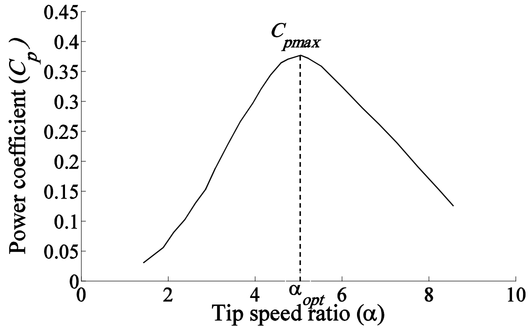

Fig. 2 Power coefficient (C_p) versus tip-speed ratio (α).

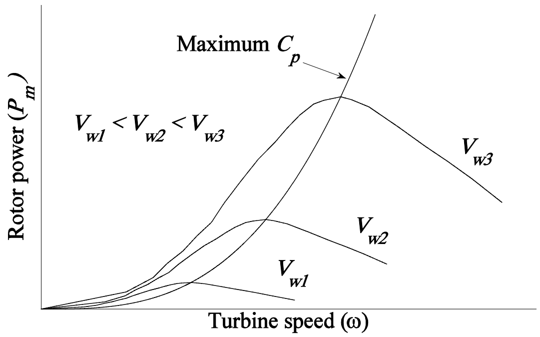

Fig. 3 Mechanical power against rotor speed for different wind speeds.

power, the rotor speed must be varied with wind speed.

Fig. 4 shows a typical power curve of wind turbine. The design of the wind turbine is such that the generation is started at the cut-in wind speed ($V_{cut\text{-}in}$) . In the maximum C_p region, the operation is at optimum value of α (α_{opt}). The output power is equal to its rated value from the rated speed (V_{rated}) to the cut-out speed ($V_{cut\text{-}out}$) [11], [13].

III. Modelling of Doubly-Fed Induction Machine

Voltage equations of the DFIG are written with the positive direction of stator currents is out of the stator terminals. These voltage equations in the stationary reference-frame are given by [14]:

$$\begin{bmatrix} u_{qs} \\ u_{ds} \\ u_{qr} \\ u_{dr} \end{bmatrix} = \begin{bmatrix} -(R_s + pL_s) & 0 & pL_m & 0 \\ 0 & -(R_s + pL_s) & 0 & pL_m \\ -pL_m & \omega_e L_m & R_r + pL_r & -\omega_e L_r \\ -\omega_e L_m & -pL_m & \omega_e L_r & R_r + pL_r \end{bmatrix} \begin{bmatrix} i_{qs} \\ i_{ds} \\ i_{qr} \\ i_{dr} \end{bmatrix} \quad (4)$$

where

$$L_s = L_{Ls} + L_m \quad (5)$$

$$L_r = L_{Lr} + L_m \quad (6)$$

$$p = \frac{d}{dt} \quad (7)$$

u_{qs}, u_{ds} q-axis and d-axis components of stator voltages
u_{qr}, u_{dr} q-axis and d-axis components of rotor voltages
ω_e electrical angular speed of induction-generator
L_s, L_r self inductances of the stator and rotor windings
i_{qs}, i_{ds} q-axis and d-axis components of stator currents
i_{qr}, i_{dr} q-axis and d-axis components of rotor currents
R_s, R_r stator and referred rotor resistances

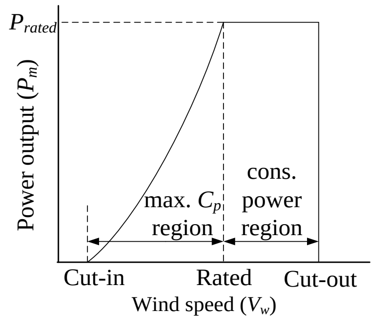

Fig. 4 Typical power curve of a wind turbine.

L_{Ls}, L_{Lr} stator and referred-rotor leakage inductances
L_m magnetizing inductance.

The equation of motion is given by

$$\frac{d\omega_m}{dt} = \frac{T_L - T_e - B_m\,\omega_m}{J} \quad (8)$$

where

$$\omega_m = \frac{\omega_e}{P} \quad (9)$$

ω_m mechanical angular speed of the DFIG
T_e electromagnetic torque of the DFIG
P number of pole pairs
T_L driving torque
B_m friction coefficient
J inertia

IV. Modeling of Battery

The lead-acid batteries can be represented by the equivalent circuit shown in Fig. 5 [6], [15], [16], where
R_c , R_d internal charge and discharge resistances
U_{bat} , U_{boc} battery terminal and open-circuit voltages
i_{bat} , C_b battery current and battery capacitance

V. Proposed Control Scheme of Stand-Alone Wind System

The proposed control scheme of the system is shown in Fig. 6. In this figure, the stator-voltage vector ($\boldsymbol{u_s}$) and stator-current vector ($\boldsymbol{i_s}$) in the stator frame, the rotor position (θ_r), and the DC-bus voltage (u_{dc}) are used to estimate the reference rotor currents $i_{Ar\text{-}ref}$, $i_{Br\text{-}ref}$ and $i_{Cr\text{-}ref}$. The differences between these reference currents and the rotor currents are the input signals to the current controllers, which are hysteresis controllers. The output signals of these controllers (A, B and C) determine the switching state of the PWM converter.

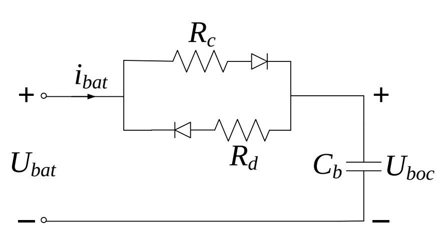

Fig. 5 Lead-cid battery equivalent circuit (directions of currents are during charging period).

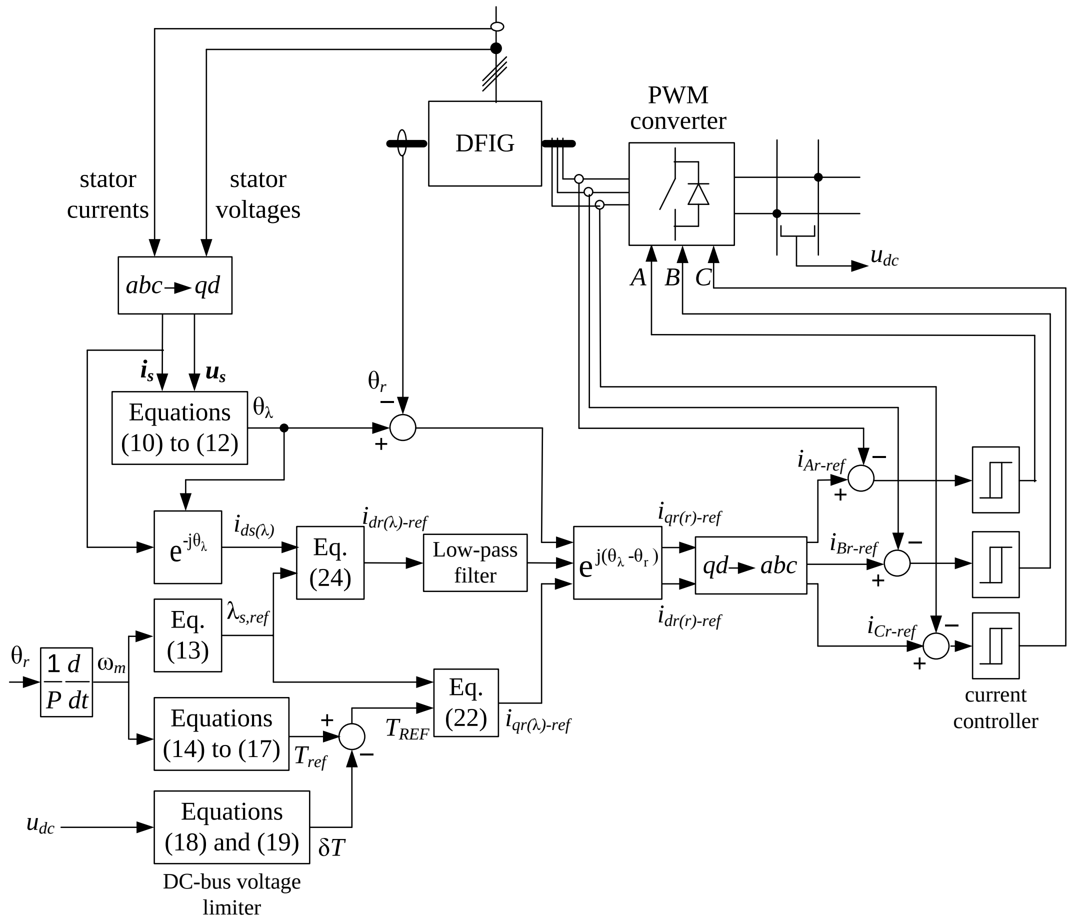

Fig. 6 Control scheme of proposed stand-alone wind system.

A. Calculation of Stator-Flux angle

The angle of the stator flux linkage (θ_λ) in the stator frame, with the positive direction of stator currents is out of the stator terminals, is determined as [17]:

$$\lambda_{qs} = \int (u_{qs} + R_s\, i_{qs})\, dt\ , \tag{10}$$

$$\lambda_{ds} = \int (u_{ds} + R_s\, i_{ds})\, dt\ , \tag{11}$$

$$\theta_\lambda = \tan^{-1}\left(\frac{\lambda_{qs}}{\lambda_{ds}}\right) \tag{12}$$

where

u_{qs}, u_{ds} q-axis and d-axis components of stator voltages
i_{qs}, i_{ds} q-axis and d-axis components of stator currents
λ_{qs}, λ_{ds} q-axis and d-axis components of stator flux linkage

B. Reference Flux and Reference Torque

The reference flux linkage is taken equal to the rated value when ω_m is less than or equal to the DFIG rated speed ($\omega_{m,\,rated}$). On the other hand, when ω_m is greater than the rated speed, the machine is operated in the field weakening region, thus:

$$\lambda_{s,ref} = \begin{cases} \lambda_{rated} & \omega_m \le \omega_{m\ rated} \\ \lambda_s\ |_{\text{rated power}} & \omega_m > \omega_{m\ rated} \end{cases} \tag{13}$$

The reference torque of the DFIG is given by:

$$T_{ref} = \frac{T_{opt}}{\text{gear ratio}} - B_m\, \omega_m \tag{14}$$

where T_{opt} is the optimal torque of the wind turbine.
The torque T_{opt} is obtained, according to Fig. 4, as follows:

$$T_{opt} = \begin{cases} \frac{1}{2} C_{p,\max}\, \rho A \left(\frac{R^3}{\alpha_{opt}^{\ 3}}\right) \omega^2 & \omega \le \omega_{opt,rated} \\ \frac{P_{rated}}{\omega} & \omega > \omega_{opt,rated} \end{cases} \tag{15}$$

$$\omega = \frac{\omega_m}{\text{gear ratio}} \tag{16}$$

where P_{rated} is the rated power of the wind turbine, ω is the turbine speed, and $\omega_{opt,rated}$ is the optimum turbine speed at rated wind speed (V_{rated}), and is given by:

$$\omega_{opt,rated} = \frac{\alpha_{opt} V_{rated}}{R} \tag{17}$$

C. DC-bus Voltage Limiter

The block "DC-bus voltage limiter" observes the battery-bank voltage, u_{dc}, to prevent this voltage from increasing above its maximum value, U_{max}. The output of this block, δT is given by:

$$\delta T = k \int b_u \, dt \qquad \delta T \geq 0 \tag{18}$$

where,

$$b_u = \begin{cases} 1 & u_{dc} > U_{\max} \\ -1 & u_{dc} \leq U_{\max} \end{cases}, \tag{19}$$

and k is the integrator gain. The value of k is determined by trial and error. In this work, k is chosen to be equal to 10.

When u_{dc} exceeds its maximum limit, b_u is set to 1 and the value of δT_e is increased. Hence, T_{REF} is decreased. Referring to Fig. 6, T_{REF} is given by

$$T_{REF} = T_{ref} - \delta T \tag{20}$$

Decreasing T_{REF} has the effect of decreasing the DFIG torque (T_e) and accelerating wind turbine beyond ω_{opt}. Operating the wind turbine beyond ω_{opt} results in less extracted power that makes u_{dc} close to U_{max}. When u_{dc} decreased below its maximum limit, i.e. b_u equal to -1, the value of δT_e is decreased. It should be noted that the value of δT_e is not allowed to go below zero.

D. Reference Rotor Currents

Firstly, reference currents are obtained in stator-flux frame as follows:

The developed torque (T_e) in the stator-flux frame can be given by [18]

$$T_e = \frac{3}{2} P \frac{L_m}{L_s} \lambda_s \, i_{qr(\lambda)} \tag{21}$$

where

$i_{qr(\lambda)}$ q-axis component of rotor current

L_s self inductance of the stator winding

L_m magnetizing inductance

The reference rotor current $i_{qr(\lambda)\text{-}ref}$ can be obtained by substituting with the values of T_{REF} and $\lambda_{s,ref}$ in (21). Thus,

$$i_{qr(\lambda)\text{-}ref} = T_{REF} \, \frac{2}{3P} \, \frac{L_s}{L_m \, \lambda_{s,ref}} \tag{22}$$

The stator flux (λ_s) in the stator-flux frame, with the positive direction of stator currents is out of the stator terminals, can be given by [14]:

$$\lambda_s = -L_s \, i_{ds(\lambda)} + L_m \, i_{dr(\lambda)} \tag{23}$$

where

$i_{ds(\lambda)}$ *d*-axis component of stator current

$i_{dr(\lambda)}$ *d*-axis component of rotor current

The reference rotor current $i_{rd(\lambda)\text{-}ref}$ can be obtained by substituting with the values of $\lambda_{s,ref}$ and $i_{ds(\lambda)}$ in (23). Thus,

$$i_{dr(\lambda)\text{-}ref} = \frac{\lambda_{s,ref} + L_s \, i_{ds(\lambda)}}{L_m} \tag{24}$$

Secondly, reference rotor currents in rotor frame ($i_{qr(r)\text{-}ref}$ and $i_{dr(r)\text{-}ref}$), where the subscript r means reference rotor frame, are obtained by using the filtered value of $i_{rq(\lambda)\text{-}ref}$ and the values of $i_{rd(\lambda)\text{-}ref}$, θ_λ and the rotor position θ_r.

Finally, reference rotor-phase currents in rotor frame ($i_{Ar\text{-}ref}$, $i_{Br\text{-}ref}$ and $i_{Cr\text{-}ref}$) are obtained by using the transformation from *qd* axes to *abc* axes.

E. Current Controller

The current controller is two-level hysteresis controller and its characteristics are shown in Fig. 7 [17]. Taking the tolerance band of this controller equal to $2H_i$, the output of this controller is given by:

$$C_{out} = \begin{Bmatrix} 1 & for \ \Delta i > H_i \\ 0 & for \ \Delta i < -H_i \end{Bmatrix}, \tag{25}$$

VI. Modes of Operation

The limiting conditions of extraction of maximum power are:

1) The DC-bus voltage never exceeds a maximum preset value.
2) The captured power from the wind turbine does not exceed the rated power of the wind turbine.

Hence, according to the battery-bank voltage (u_{dc}), we have two modes of operation. Mode 1 is when $u_{dc} \leq U_{max}$, and Mode 2 is when $u_{dc} > U_{max}$. Fig. 8 illustrates these operating modes.

In Mode 1 of operation, the required operation of the system is according to the power curve of the wind turbine, Fig. 4. This mode is explained in Fig. 9.

In Mode 1(A), it is required to capture the maximum power from cut-in to rated wind speeds as shown in Fig. 9(a). In this figure, the wind speed is increased from V_{w1} to V_{w2} where $V_{w2} \leq V_{rated}$, and the captured power follows the path *X-Y-Z*.

In Mode 1(B), it is required to capture the rated power from rated to cut-out wind speeds as shown in Fig. 9(b). In this figure, the wind speed is increased from V_{w1} to V_{w2} where $V_{w2} > V_{rated}$.

In Mode 2 of operation, the turbine is accelerated beyond ω_{opt} to operate at the power that makes u_{dc} equals U_{max}. This power is less than the captured power in Mode 1 for the same wind speed. This mode is explained by Fig. 10. The captured power follows the path *X-Y-Z.*

VII. Simulation of Proposed Stand-Alone Wind System

The system is simulated using MATLAB/SIMULINK [19]. Data of DFIG, wind turbine and battery bank are given in

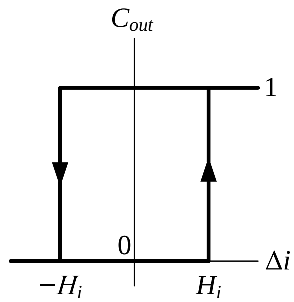

Fig. 7 Characteristics of current controller

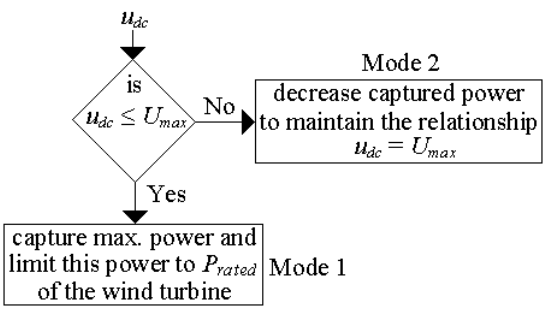

Fig. 8 Modes of operation.

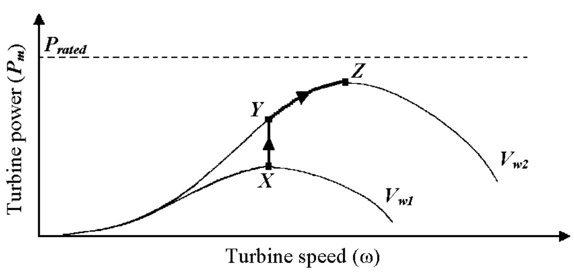

(a) Mode 1(A)

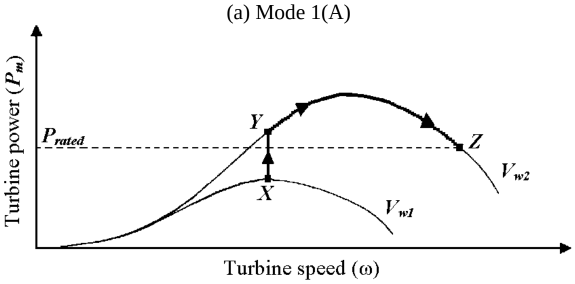

(b) Mode 1(B)

Fig. 9 Mode 1 of operation.

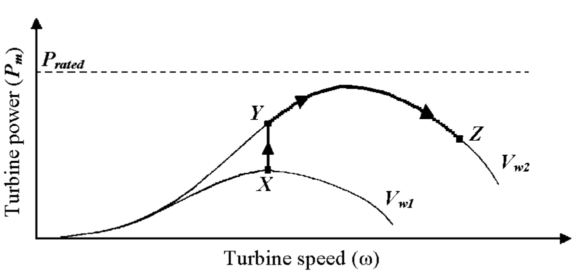

Fig. 10 Mode 2 of operation.

the Appendix. A capacitor filter of 10 mF is connected across the battery bank to reduce the ripple currents. Rectifier states are reviewed every about 71 μsec. This means that each of the turn-on and turn-off times of the rectifier switches has minimum value of about 71 μsec and, hence, the maximum switching frequency is about 7 kHz. The low-pass filter has cutoff frequency of 1 kHz. The load connected to the DC-bus, Fig. 1, is considered a resistive load and its value is R_L .

To study Mode 1, state of charge (*SOC*) of the battery bank is chosen of low value to operate at $u_{dc} < U_{max}$.

For Mode 1(A), where $V_{w2} \leq V_{rated}$, results for *SOC* = 0.3, R_L = 12 Ω and wind speed (V_w) changed suddenly from 4 m/s ($V_{cut\text{-}in}$) to 11.5 m/s (V_{rated}) at time equal to 2 s are shown in Figs. 11 to 14. Fig. 11 shows that the captured power from the wind turbine is increased gradually, starting from the time of change of wind speed, until maximum power operation is obtained. The steady-state captured power is about 3681 watt, while the optimal maximum power is equal to the rated power of the wind turbine which is 3694 watt. Therefore, the captured power has about 0.35 % deviation, and good peak-power operation is obtained. Fig. 11, also, shows that the turbine speed is increased gradually to the value corresponding to maximum power operation. The steady-state turbine speed is about 301 rpm, while the optimal turbine speed corresponding to optimal maximum power is about 299 rpm. Therefore, the turbine speed has about -0.7 % deviation. Fig. 12 shows that the DC-bus voltage is less than its maximum limiting value (U_{max}), where U_{max} is about 130.39 V, confirming Mode 1(A) of operation. Figs. 13 and 14 show that the steady-state stator and rotor phase currents of the DFIG are nearly sinusoidal currents with total-harmonic distortion (THD) of about 6.2 % and 5.4 % respectively. This is achieved by incorporating a low-pass filter in the control scheme. It should be noted that the removing of the low-pass filter increases the distortion of stator and rotor currents as shown in Figs. 15 and 16 respectively.

For Mode 1(B), where $V_{w2} > V_{rated}$, results for *SOC* = 0.3, R_L = 12 Ω and wind speed (V_w) changed suddenly from 11.5 m/s (V_{rated}) to 15 m/s at time equal to 2 s are shown in Figs. 17 and 18. Fig. 17 shows that the captured power from the wind turbine is increased beyond rated power of the turbine, starting from the time of change of wind speed, until rated power operation is obtained. The steady-state captured power is about 3618 watt, while the rated power is equal to 3694 watt. Therefore, the captured power has about 2.1 % deviation, and good rated power operation is obtained. Fig. 17, also, shows that the turbine speed is increased gradually to turbine speed corresponding to rated power operation. The steady-state turbine speed is about 622 rpm, while the required turbine speed corresponding to rated power operation is about 619 rpm. Therefore, the turbine speed has about -0.49 % deviation. Fig. 18 shows that the DC-bus voltage is less than its maximum limiting value, confirming Mode 1(B) of operation.

Different values of volt-ampere of PWM converter corresponding to different wind speeds are estimated. The results are obtained for *SOC* = 0.3, R_L = 12 Ω, and are given in TABLE I. These results show that the power rating of the PWM converter is less than 60 % of the rated power of wind turbine for our system. Therefore, the cost of the system is reduced.

TABLE I
POWER OF PWM CONVERTER FOR DIFFERENT WIND SPEEDS

Wind speed (m/s)	4	6	8	10	11.5	13	15	17	20
Power (kVA)	0.57	0.8	1.15	1.62	2.04	1.95	1.89	1.85	1.78

To study Mode 2, *SOC* of the battery bank is chosen of high value to make the value of u_{dc} increases to U_{max} . Results for *SOC* = 0.9, R_L = 12 Ω and wind speed (V_w) changed suddenly from 4 m/s ($V_{cut\text{-}in}$) to 11.5 m/s (V_{rated}) at time equal 2 s are shown in Figs. 19 and 20. Fig. 19 shows that the captured power from the wind turbine is increased gradually, starting from the time of change of wind speed, and crossing its maximum value. Finally, the captured power from the wind turbine is at a value that makes u_{dc} equal to U_{max} . Fig. 20 shows the DC-bus voltage with steady-state mean value of about 130.387 V, while the maximum DC-bus voltage is about 130.39 V. Therefore, the mean DC-bus voltage has about 0.002 % deviation, and good maximum voltage operation is obtained.

It should be noted that the reduction of captured power shown in Fig. 19 will decrease if the system supplies higher loads. To explain this condition, it is assumed that the system was operating at the conditions described in Fig. 19, then the load is increased (R_L decreased) from 12 Ω to 6 Ω at time equal to 2 s. Fig. 21 shows that the captured power from the wind turbine is increased gradually until maximum power operation is obtained. The steady-state captured power is about 3674 watt, while the optimal maximum power is 3694 watt. Therefore, the captured power has about 0.54 % deviation, and a good peak-power operation is obtained. Fig. 21, also, shows that the turbine speed is decreased gradually to the value corresponding to maximum power operation. The steady-state turbine speed is about 302rpm, while the optimal turbine speed corresponding to optimal maximum power is about 299 rpm. Therefore, the turbine speed has about -1 % deviation. Fig. 22 shows that the DC-bus voltage is decreased and becomes less than its maximum value (U_{max}), where U_{max} is about 130.39 V, which is Mode 1(A) of operation.

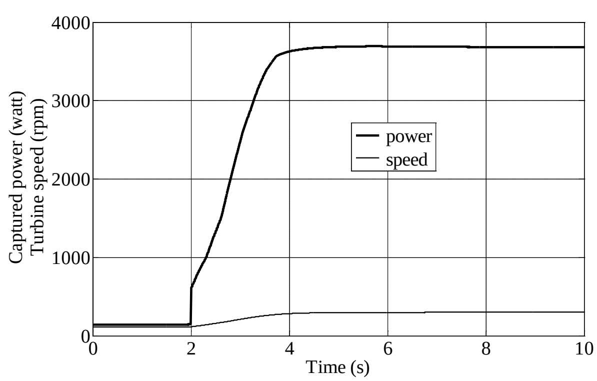

Fig. 11 Captured power of the wind turbine and turbine speed for *SOC* = 0.3, R_L = 12 Ω and V_w changed from 4 m/s to 11.5 m/s at t = 2 s (Mode 1(A)).

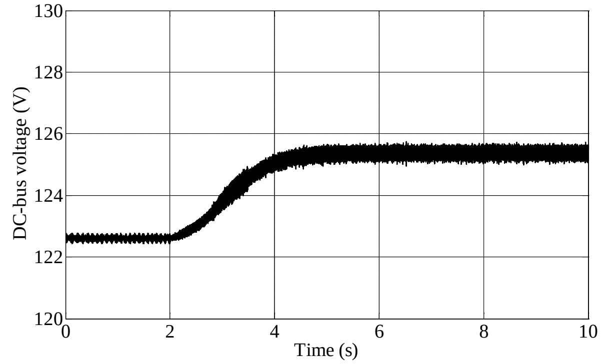

Fig. 12 DC-bus voltage for *SOC* = 0.3, R_L = 12 Ω and V_w changed from 4 m/s to 11.5 m/s at t = 2 s (Mode 1(A)).

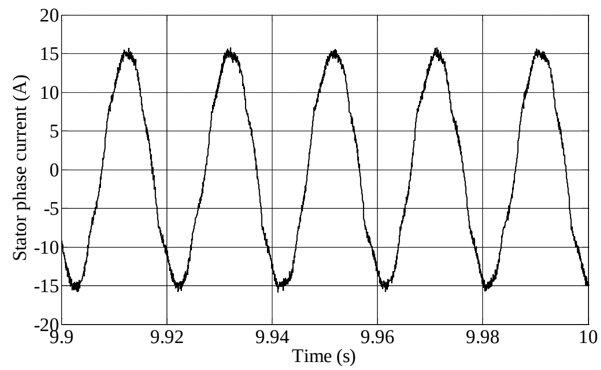

Fig. 13 Steady-state stator-phase current of the DFIG for *SOC* = 0.3, R_L = 12 Ω and V_w changed from 4 m/s to 11.5 m/s at t = 2 s (Mode 1(A)).

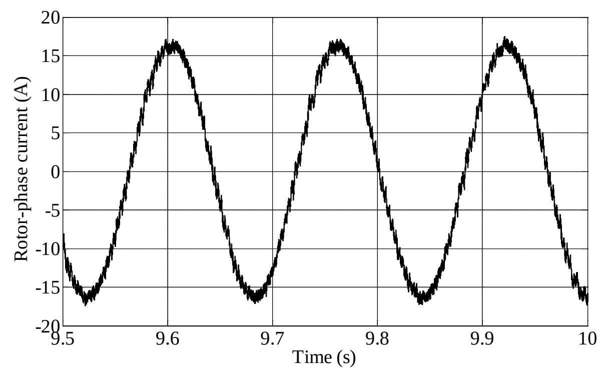

Fig. 14 Steady-state Rotor-phase current of the DFIG for *SOC* = 0.3, R_L = 12 Ω and V_w changed from 4 m/s to 11.5 m/s at t = 2 s (Mode 1(A)).

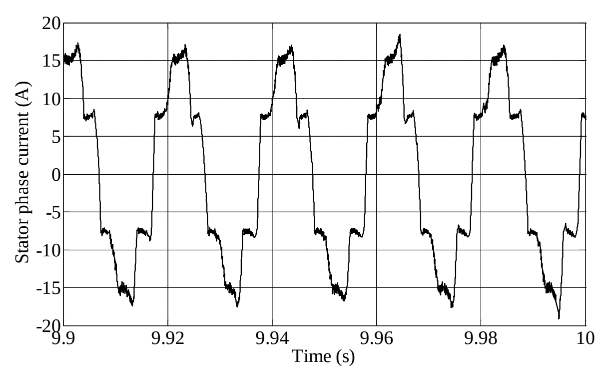

Fig. 15 Steady-state stator-phase current of the DFIG after removing the low-pass filter for *SOC* = 0.3, R_L = 12 Ω and V_w changed from 4 m/s to 11.5 m/s at t = 2 s (Mode 1(A)).

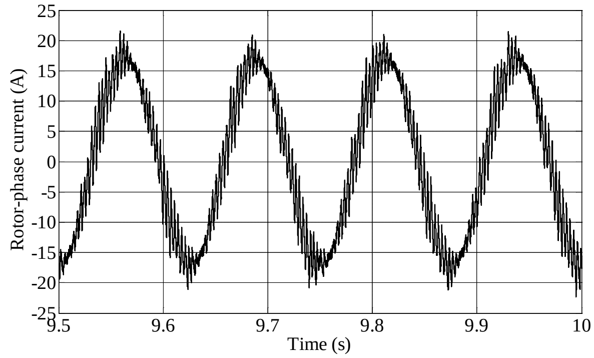

Fig. 16 Steady-state Rotor-phase current of the DFIG after removing the low-pass filter for *SOC* = 0.3, R_L = 12 Ω and V_w changed from 4 m/s to 11.5 m/s at t = 2 s (Mode 1(A)).

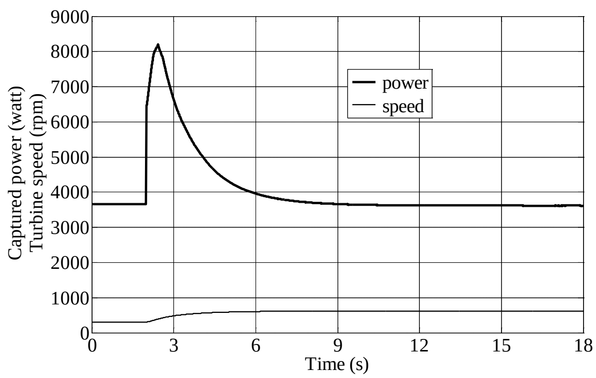

Fig. 17. Captured power of the wind turbine and turbine speed for *SOC* = 0.3, R_L = 12 Ω and V_w changed from 11.5 m/s to 15 m/s at t = 2 s (Mode 1(B)).

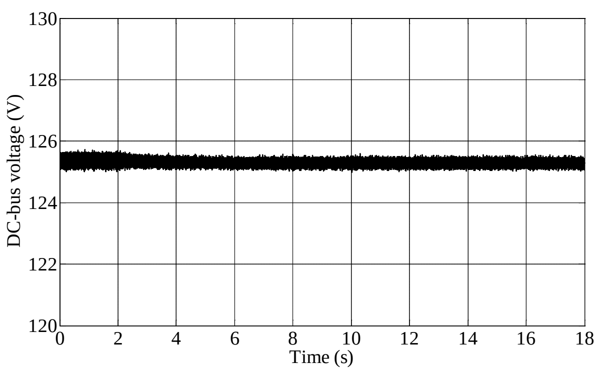

Fig. 18 DC-bus voltage for *SOC* = 0.3, R_L = 12 Ω and V_w changed from 11.5 m/s to 15 m/s at t = 2 s (Mode 1(B)).

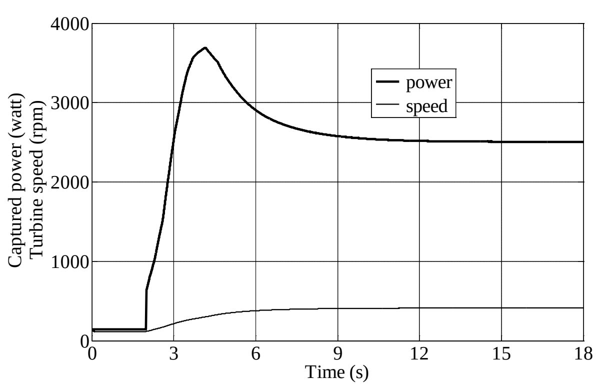

Fig. 19 Captured power of the wind turbine and turbine speed for *SOC* = 0.9, R_L = 12 Ω and V_w changed from 4 m/s to 11.5 m/s at t = 2 s (Mode 2).

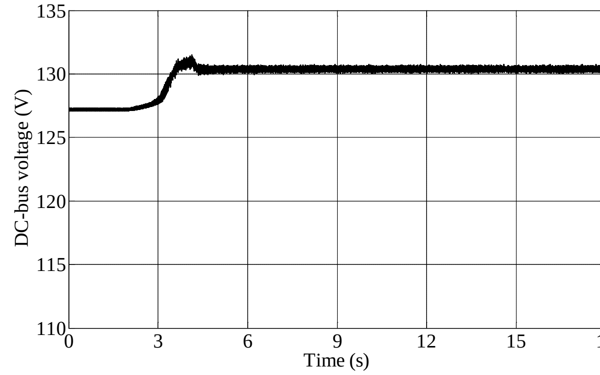

Fig. 20 DC-bus voltage for *SOC* = 0.9, R_L = 12 Ω and V_w changed from 4 m/s to 11.5 m/s at t = 2 s (Mode 2).

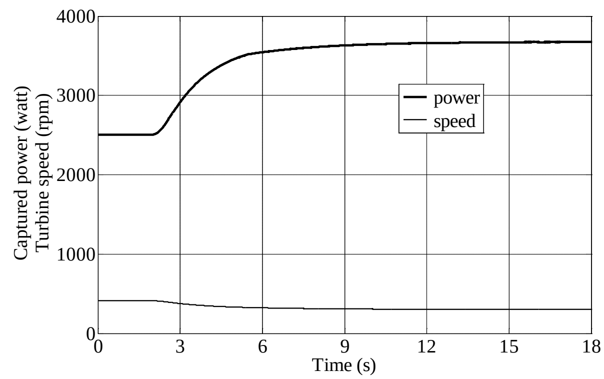

Fig. 21 Captured power of the wind turbine and turbine speed for *SOC* = 0.9, V_w = 11.5 m/s and R_L decreased from 12 Ω to 6 Ω at t = 2 s (Mode 1(A)).

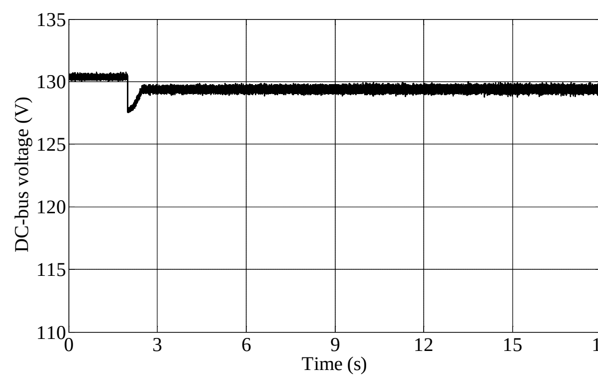

Fig. 22 DC-bus voltage for *SOC* = 0.9, V_w = 11.5 m/s and R_L decreased from 12 Ω to 6 Ω at t = 2 s (Mode 1(A)).

It should be noted that the voltage u_{dc} reaches its maximum voltage limit (U_{max}) although the battery bank is not fully charged. This is due to the internal resistance of the battery bank. However, *SOC* will increase gradually to full-charge state.

VIII. Conclusion

The proposed stand-alone wind system with battery storage using DFIG is studied. In addition to using DFIG, the proposed system has PWM converter with low power rating. Therefore, the system is of low cost compared with the traditional system. The main objective of the PWM converter control is to capture the maximum possible power from the wind turbine as long as the rated power of the wind turbine and the maximum voltage limit of the battery bank are not violated. Also, the reactive power required by DFIG is obtained from the battery bank through the controlled PWM converter. According to the battery-bank voltage (u_{dc}), there are two modes of operation of the system. One mode when the battery-bank voltage is less than or equal to the maximum voltage limit, and the other mode when the battery-bank voltage exceeds the maximum voltage limit. In the first mode, maximum power from the wind turbine is captured, and this power is limited to the rated power of the wind turbine. In the second mode, the captured power is less than that power obtained in the first mode for the same wind speed such that the battery bank voltage is limited to its maximum value. Modeling and control of the system are demonstrated. Various operating conditions have been considered in the paper to verify the capability of the proposed system.

REFERENCES

[1] W. Qi, J. Liu, X. Chen, and P. D. Christofides, "Supervisory predictive control of standalone wind/solar energy generation systems," IEEE Trans. Control Systems Technology, vol. 19, no. 1, pp. 199–207, Jan. 2011.

[2] L.-Q. Liu and Z.-X. Wang, "The development and application practice of wind-solar energy hybrid generation systems in China," Renewable and Sustainable Energy Reviews, no. 13, pp. 1504–1512, 2009.

[3] F. Valenciaga and P. F. Puleston, "High-order sliding control for a wind energy conversion system based on a permanent magnet synchronous generator," IEEE Trans. Energy Conversion, vol. 23, no. 3, pp. 860–867, Sep. 2008.

[4] B. S. Borowy and Z. M. Salameh, "Dynamic response of a stand-alone wind energy conversion system with battery energy storage to a wind gust," IEEE Trans. Energy Conversion, vol. 12, no. 1, pp. 73–78, March 1997.

[5] E. Koutroulis and K. Kalaitzakis, "Design of a maximum power tracking system for wind-energy-conversion applications," IEEE Trans. Ind. Electron., vol. 53, no. 2, pp. 486–494, April 2006.

[6] M. H. Nehrir, B. J. LaMeres, G. Venkataramanan, V. Gerez, and L. A. Alvarado, "An approach to evaluate the general performance of stand-alone wind/photovoltaic generating systems," IEEE Trans. Energy Conversion, vol. 15, no. 4, pp. 433–439, Dec. 2000.

[7] J. P. Dunlop, "Batteries and charge control in stand-alone photovoltaic systems, fundamentals and application," Report, Sandia National Laboratories, Photovoltaic systems Applications Dept., Jan. 1997.

[8] H. Polinder, F. F. A. van der Pijl, G.-J. de Vilder, and P. J. Tavner, "Comparison of direct-drive and geared generator concepts for wind turbines," IEEE Trans. Energy Conversion, vol. 21, no. 3, pp. 725–733, Sep. 2006.

[9] O. E. S. Mohammed, N. M. B. Abdel-Rahim, and A. Shaltout, "Stand-alone wind system with battery storage using induction generator and direct torque control," in Proc. MEPCON' 2009, 13th Middle East Power Systems Conf., Assuit University, Egypt, pp. 50–56, Dec. 2009.

[10] A. M. De Broe, S. Drouilhet, and V. Gevorgian, "A peak power tracker for small wind turbines in battery charging applications," IEEE Trans. Energy Conversion, vol. 14, no. 4, pp. 1630–1635, Dec. 1999.

[11] M. R. Patel, "Wind and solar power systems," Book, CRC Press, 1999.

[12] D. S. Zinger and E. Muljadi, "Annualized wind energy improvement using variable speeds," IEEE Trans. Ind. Applicat., vol. 33, no. 6, pp. 1444–1447, Nov./Dec. 1997.

[13] R. Karki and R. Billinton, "Reliability/cost implication of PV and wind energy utilization in small isolated power systems," IEEE Trans. Energy Conversion, vol. 16, no. 4, pp. 368–373, Dec. 2001.

[14] P. C. Krause, O. Wasynczuk, and S. D. Sudhoff, "Analysis of electric machinery and drive systems," Book, IEEE Press, Second Edition, 2002.

[15] Z. M. Salameh, M. A. Casacca, and W. A. Lynch, "A mathematical model for lead-acid batteries," IEEE Trans. Energy Conversion, vol. 7, no. 1, pp. 93–98, March 1992.

[16] Y.-H. Kim and H.-D. Ha, "Design of interface circuits with electrical battery models," IEEE Trans. Ind. Electron., vol. 44, no. 1, pp. 8–16, Feb. 1997.

[17] A. M. Trzynadlowski, "Control of induction motors," Book, Academic Press, 2001.

[18] L. Xu, D. Zhi, and B. W. Williams, "Predictive current control of doubly fed induction generators," IEEE Trans. Ind. Electron., vol. 56, no. 10, pp. 4143–4153, Oct. 2009.

[19] SIMULINK 7, The MathWorks, Inc., 2007.

[20] R. Perez, "Lead-acid battery state of charge vs. voltage," Home Power, no. 36, pp. 66–69, Aug./Sep. 1993.

APPENDIX

The machine used in this paper is:
Δ-connected, 3.73 kW, $220/\sqrt{3}$ V, 20.8 A, 1712 rpm, 4 poles, 60 Hz wound-rotor induction machine, and has the following parameters:
R_s = 0.45 Ω, R_r = 0.5 Ω, L_{ls} = 3.0 mH, L_{lr} = 3.0 mH, L_m = 110.0 mH and turns ratio = 1.0 .

The wind turbine used in this paper is 3.694 kW, horizontal-axis wind turbine, and has the following parameters:
R = 1.85 m, V_{cutin} = 4 m/s, V_{rated} = 11.5 m/s, V_{cutout} = 20 m/s, and has C_p–α characteristics shown in Fig. 2.
Total inertia = 0.15 kg.m^2, total friction coefficient = 0.001 N.m.s/rad, and gear ratio = 5.72.

The battery bank used in this paper is 120 V, two parallel branches banks are used. Each branch consists of ten batteries. Each battery is 12 V, 175 Ah deep-cycle, lead-acid battery, and has characteristics derived from measured data [20]. The derived characteristics are given in the TABLE II. The maximum voltage limit of one battery is U_{boc} at SOC = 1 which is equal to 13.039 V.

TABLE II
BATTERY PARAMETERS

Equivalent circuit parameters	State of charge (*SOC*)	
	0.3	0.9
U_{boc} (V)	12.401	12.804
R_c (Ω)	0.0172	0.0712
R_d (Ω)	0.0304	0.0174